RESEARCH ARTICLE

Key Points:
- The 410 and 660 km seismic discontinuities beneath the Korea and SW Japan are imaged
- They are affected by various factors as well as temperature of the slab

Correspondence to:
J. Rhie,
rhie@snu.ac.kr

Topography of the 410 and 660 km discontinuities beneath the Korean Peninsula and southwestern Japan using teleseismic receiver functions

Sang-Hyun Lee[1,2], Junkee Rhie[2], Yongcheol Park[1], and Kwang-Hee Kim[3]

[1]Korea Polar Research Institute, Incheon, South Korea, [2]School of Earth and Environmental Sciences, Seoul National University, Seoul, South Korea, [3]Department of the Geological Sciences, Pusan National University, Busan, South Korea

Abstract Topography of the 410 and 660 km seismic upper mantle discontinuities beneath the Korean Peninsula and southwestern Japan were determined using teleseismic receiver functions. *P* receiver functions were migrated from delayed times to corresponding piercing (conversion) points of *P*-to-*S* converted phases, using one-dimensional (1-D) and three-dimensional (3-D) models. Receiver functions were then stacked using Common Conversion Point (CCP) techniques, to enhance signal-to-noise ratios and thereby reduce uncertainty (noise). The 410 and 660 km discontinuities were clearly imaged, as positively valued amplitude peaks of CCP stacked receiver functions in the study area. Topographic variations were roughly consistent with the low temperature of the subducting Pacific Plate. However, the complex structure of the subducting Pacific Plate produced distinct changes of upper mantle discontinuities, which cannot be explained by temperature variations alone. Depression of the 410 km discontinuity, observed in a wide region extending from the Korean Peninsula to Kyushu Island, may be related to trench rollback history. Furthermore, the topography of the 660 km discontinuity varies significantly with latitude. At latitudes higher than 38°N, its depth remains unchanged, despite the presence of the stagnant slab, while significant depression has been observed at latitudes below 36°N. This may have been caused by differences in the angles of subduction of the Japan slab and the Izu-Bonin slab. However, heterogeneity of the water content of slabs may also have contributed to this topographical difference.

1. Introduction

Studying depth variations of the 410 and 660 km seismic discontinuities—hereafter referred to as the 410 and the 660, respectively—beneath the Korean Peninsula and the surrounding regions is important, as it helps to increase understanding of the effects of cold slabs on upper mantle discontinuities. The 410 and the 660 are well-established upper mantle discontinuities, from seismological and mineral physical perspectives. They have been detected around the globe and generally explained by a series of phase transformations of olivine: olivine to wadsleyite (β-spinel) for the 410 and ringwoodite (γ-spinel) to perovskite + magnesiowüstite for the 660 [*Ringwood*, 1975; *Ita and Stixrude*, 1992]. The layer in between the 410 and the 660 is defined as the Mantle Transition Zone (MTZ). Inside the MTZ, another discontinuity was observed in some regions, at a nominal depth of 520 km, attributable to the phase transformation of wadsleyite to ringwoodite [*Shearer*, 1996]. Although exact depths of phase transformations locally vary with temperature, the type of change is determined by the Clapeyron slope. The Clapeyron slope is positive for the phase transition of olivine-to-wadsleyite [*Morishima et al.*, 1994], indicating that the 410 will be elevated in a cold region such as a subduction zone. However, the Clapeyron slope is negative for the postspinel transformation [*Ito and Takahashi*, 1989], indicating that the 660 will be depressed in such a region. Although it is well known that the 660 can play a role in interrupting slabs from descending into the lower mantle [*Ringwood*, 1994], how slabs are affected in detail significantly varies from place to place.

The Pacific Plate is subducting underneath the North America (or Okhotsk) Plate at the Japan Trench and underneath the Philippine Sea Plate at the Izu-Bonin Trench, respectively, with varying convergence rates and slopes. While the Japan slab, subducting westward at the Japan Trench, has a gentle slope and reaches a depth of 660 km beneath the eastern coast of the Korean Peninsula, the Izu-Bonin slab, subducting in southwest direction at the Izu-Bonin Trench, has a steeper slope and already reaches this depth beneath Kyushu Island, Japan [*Gudmundsson and Sambridge*, 1998] (Figure 1a). Furthermore, tomographic images of seismic high-velocity anomalies from previous studies clearly showed that the Japan and Izu-Bonin slabs penetrate the 410, while they
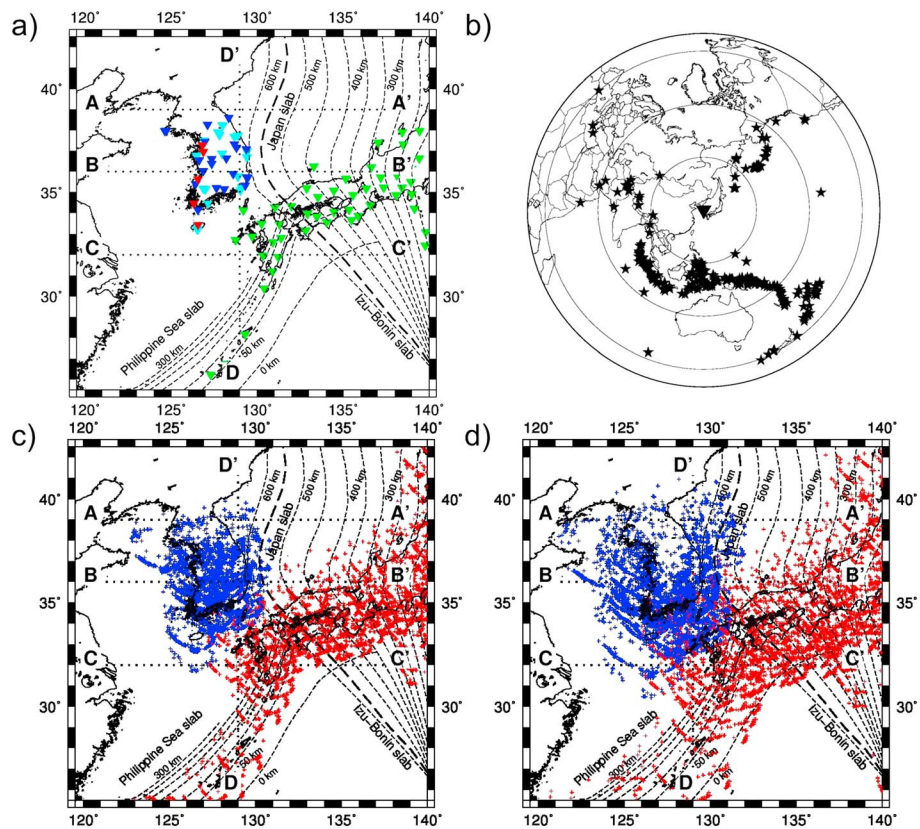
Figure 1. (a) Distribution of the Korea Meteorological Administration (KMA) (cyan and red), the Korea Institute of Geoscience and Mineral Resources (KIGAM) (blue), and Full Range Seismograph Network of Japan (F-net) (green) stations used in this study. The dashed contour lines represent the isodepths of the subducting Pacific Plate (Japan slab and Izu-Bonin slab) and Philippine Sea Plate (Philippine Sea slab) with 50 km intervals [*Gudmundsson and Sambridge*, 1998]. Dotted lines (AA'–DD') are profile lines of CCP stacked receiver function sections. (b) Distribution of events used in this study, centered at (36.5°N, 128.0°E). Epicentral distances of 30°, 60°, and 90° from the center are given by the concentric circles with smallest, intermediate, and largest radius, respectively. (c) Location of the conversion points of P410s phases recorded at the Korean Peninsula (blue) and Japan Islands (red). (d) Same as Figure 1c, but for the P660s phases.

tend to flatten out over the 660 [*Mégnin and Romanowicz*, 2000; *Huang and Zhao*, 2006]. From this, it can be inferred that these slabs are not directly descending into the lower mantle in this specific region. Furthermore, *Obayashi et al.* [2009] argued that the two slabs are torn apart at their junction below a depth of 300 km.

The depth variations of the 660 in northeast Asia, determined from long-period SS precursors [*Shearer and Masters*, 1992], are in good agreement with tomographic images, indicating broad depression resulting from the cold—flat-lying—slab inferred from the high-velocity anomalies in tomographic images. However, several other regional studies using receiver functions have reported otherwise. The receiver function image obtained from broadband seismic stations in Japan, and from some stations in Korea and China, shows a local depression of the 660 beneath northeast China, where the northern part of the Japan slab reaches the 660 [*Li et al.*, 2000]. Moreover, *Li and Yuan* [2003] reported similar results, recorded by a regional network of receiver functions in northeastern China. They proposed that the northern part of the Japan slab locally penetrates the 660, where slab material has accumulated. However, the spatial sample coverage of the depressed 660 may not be sufficient, due to the limited number of stations, especially to the south. In the same region, multiple discontinuities have been reported around the depressed 660, by yet another receiver function study [*Ai et al.*, 2003]. These multiple discontinuities might be explained by phase transformations of nonolivine components in the upper mantle [e.g., *Simmons and Gurrola*, 2000], although the possibility that this discontinuity was formed by multiple reflections of shallower discontinuities of the mantle cannot be ruled out [*Li and Yuan*, 2003].

To better understand the complex interactions between upper mantle discontinuities and the subducting Japan slab and Izu-Bonin slab, detailed topographic maps of the 410 and the 660 beneath the Korean

Peninsula and the surrounding regions are of great importance. In this study, we present for the first time, high-resolution receiver function images of the MTZ beneath the Korean Peninsula, using the Common Conversion Point (CCP) stacking method. Our image also includes the MTZ beneath southwestern Japan. Broadband seismic networks were used to produce a high-resolution receiver function image, and it complements other images obtained from previous studies for northeast China [*Li and Yuan*, 2003], east China [*Ai and Zheng*, 2003], and Japan [*Niu et al.*, 2005].

2. Data and Methods

Broadband waveforms were obtained from the Korea National Seismic Network (KNSN), operated by the Korea Meteorological Administration (KMA), the Korea Institute of Geoscience and Mineral Resources (KIGAM), and temporary stations installed by the Korea Ocean Research and Development Institute (KORDI). The histories and instrumental information of KNSN and KIGAM network are well described in a previous study [*Park et al.*, 2010]. The KORDI temporary seismic network consists of six stations, unevenly distributed over the western coastline of South Korea, with broadband seismometers (Guralp CMG-3T and Reftek RT 130 data logger). We also included data recorded by F-net broadband seismic stations [*Matsumoto et al.*, 2006] in southwestern Japan to expand our receiver function image and to validate our results by comparison with previous receiver function results for the same region [*Niu et al.*, 2005]. The total number of stations used in this study is 123, but the number of stations used for individual events varies (Figure 1a).

We collected waveforms for 624 teleseismic events recorded by stations. To obtain a clear receiver function image, we selected events of $> M_w$ 6.0 and epicentral distances ranging between 30° and 90°. This is because waveforms can be complex due to upper mantle triplications and P wave diffractions along the core mantle boundary, for epicentral distances not within this range. To avoid low signal-to-noise ratio and P waveform complexity due to complex rupture processes, we used each waveform that had a direct P phase signal of clear and simple shape. In total, 328 events were selected, providing a good azimuthal distribution although events with back azimuths between 0° and 90° are relatively rare (Figure 1b).

Radial receiver functions were estimated by deconvolving radial components from vertical components using the iterative time domain deconvolution method [*Ligorria and Ammon*, 1999]. Out of the vast set of more than 13,000 receiver functions, ~5200 receiver functions remained for further analysis, after removing noisy receiver functions. To remove noisy receiver functions, we first removed those with completeness of less than 80%. Here completeness is defined as the cross-correlation coefficient between two radial component waveforms. One is the observed radial component waveform, and the other is the predicted radial component waveform obtained by convolution of the vertical component waveform and the radial receiver function. Then, those anomalous receiver functions with highly oscillating wiggles or large low-frequency noise were manually excluded. To enhance the generally low signal-to-noise ratio of P-to-S converted phases and thus produce clearer images of upper mantle discontinuities, we CCP stacked the receiver functions [*Owens et al.*, 2000]. For all station event pairs, theoretical travel times and piercing (conversion) points of possible P-to-S phases were calculated for both 1-D and 3-D models, at predefined conversion depths between 5 and 900 km, at 5 km intervals. The IASP91 [*Kennett and Engdahl*, 1991] is used as the 1-D model, and the 3-D model is constructed by combining the CRUST2.0 [*Bassin et al.*, 2000] and GAP-P2 [*Obayashi et al.*, 2009] models.

We migrated receiver functions from delayed times to corresponding piercing (conversion) points, by calculation of theoretical travel time differences between direct P waves and P-to-S converted phases at every depth interval, enabling us to map the amplitudes of receiver functions at piercing (conversion) points of P-to-S converted phases. Two-dimensional grid cells with a lateral spacing of 0.25° were predefined at each depth, and amplitudes of receiver functions at corresponding piercing points within 1.0° circular bins around grid points were linearly stacked. The 1.0° circular bin size was selected after testing several bin sizes. With bin sizes of 0.25° and 0.5°, coherent signals were not observed because the number of receiver functions was insufficient to suppress the noise, whereas larger bin sizes reduced the resolving power. Therefore, we decided to use the bin size of 1.0° based on considerations of stability and resolution. After CCP stacking, receiver functions could be regarded as good approximations to zero-offset data (zero source–receiver distance). Moreover, stacked amplitudes could be regarded as good approximations of the amplitudes of P-to-S converted phases at their piercing points, i.e., at the discontinuities responsible for these conversions (Figures 1c and 1d). To avoid distortions that occur when noise is not muted due to an insufficient number of receivers, we removed stacked amplitudes
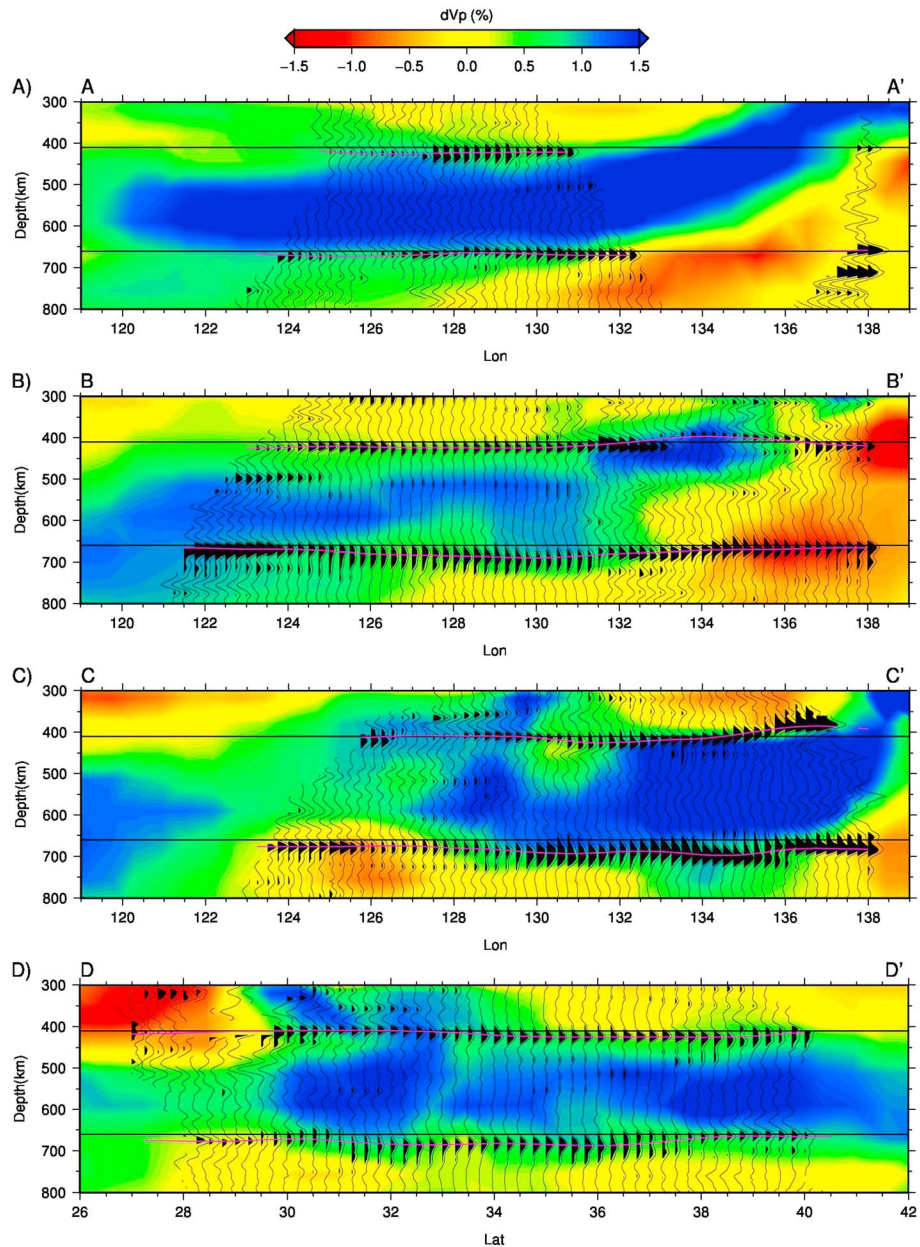
Figure 2. CCP stacked receiver function sections based on the IASP91 1-D velocity model for profile lines AA'–DD'. The positive amplitudes of up to 2 sigma error bounds from the mean are shaded in black. The mean and 2 sigma error bounds are derived from bootstrapping. The background color spectrum from blue to red represents fast to slow *P* wave velocity structure anomalies, respectively, from the GAP-P2 model [*Obayashi et al.*, 2009].

when the number of stacked receiver functions was less than 20. The depths of both the 410 and the 660 were determined by selecting the dominant peaks at corresponding depths for each grid point. In some regions, multiple peaks were observed near the depths of 410 and 660 km. However, we did not investigate these multiple peaks further. Moreover, only dominant peaks were assumed to give reliable depth estimates of the corresponding discontinuity. However, when multiple peaks had too similar amplitudes, the dominant peak caused unstable sequences of detection, resulting in—locally—unrealistic imaging of the topography of the 410 and the 660. To reduce this effect, we applied a spatial moving average on the determined depths of the 410 and the 660 for smoothing of the topography. In addition to multiple peaks, negative peaks were also observed in the vicinities of the discontinuities, especially above the 410. These negative signals could be related to partial melting at the top of the 410 [*Song et al.*, 2004]. Although the investigation of negative peaks is
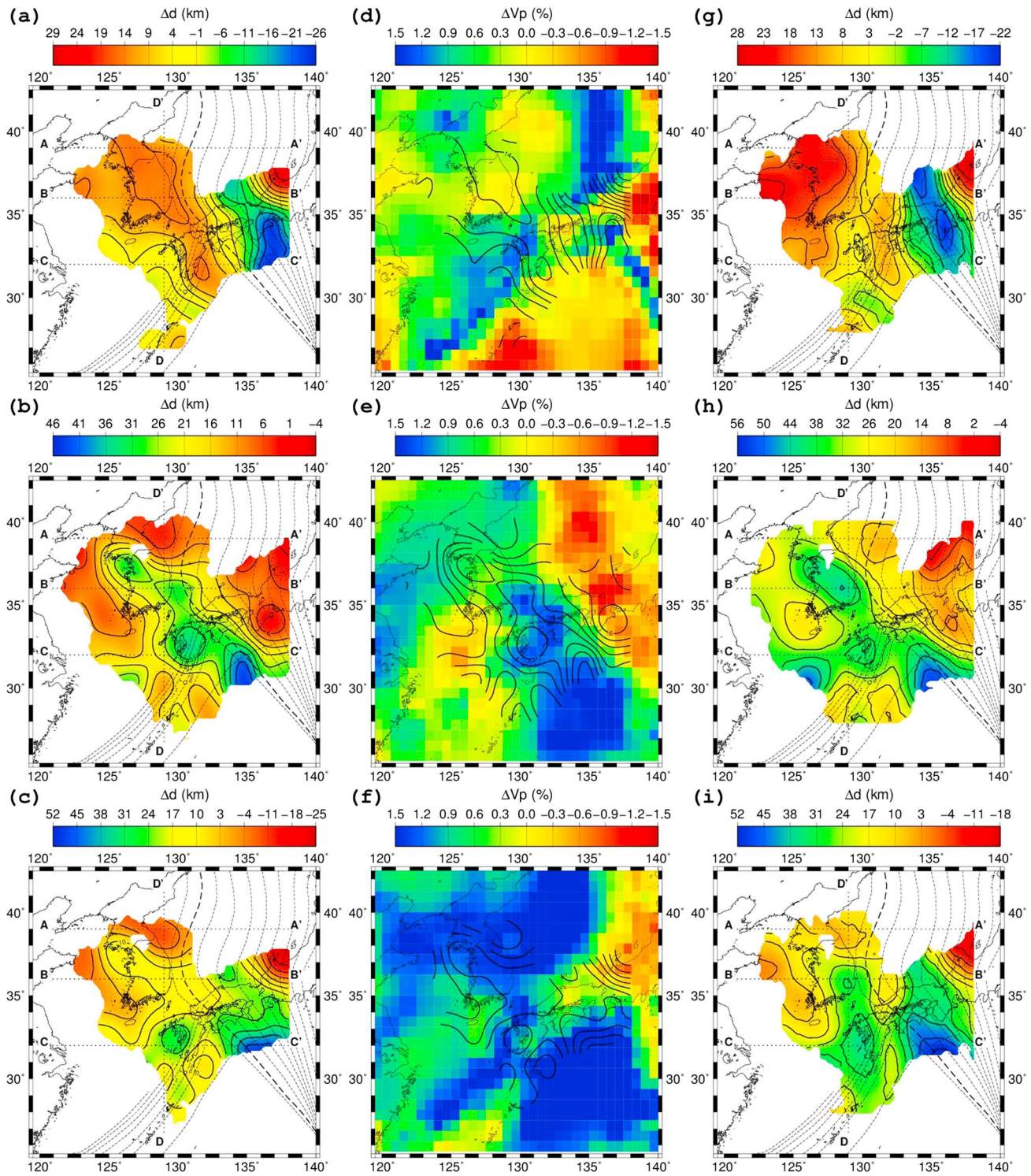
Figure 3. (a) The topography of the 410, (b) topography of the 660, and (c) variation of the MTZ thickness determined with the IASP91 1-D velocity model. The velocity perturbation at the corresponding depths to (d) the 410, (e) the 660, and (f) the MTZ thickness from GAP-P2 [*Obayashi et al.*, 2009] with contour lines of the topography. (g) The topography of the 410, (h) topography of the 660, and (i) variation of the MTZ thickness determined with the 3-D velocity model. The colors represent the perturbation of depth with respect to 410 km (Figures 3a and 3g) and to 660 km (Figures 3b and 3h), or of thickness with respect to 250 km (Figures 3c and 3i). Contour lines of topography are drawn with intervals of 10 km. Others are the same as Figure 1a.
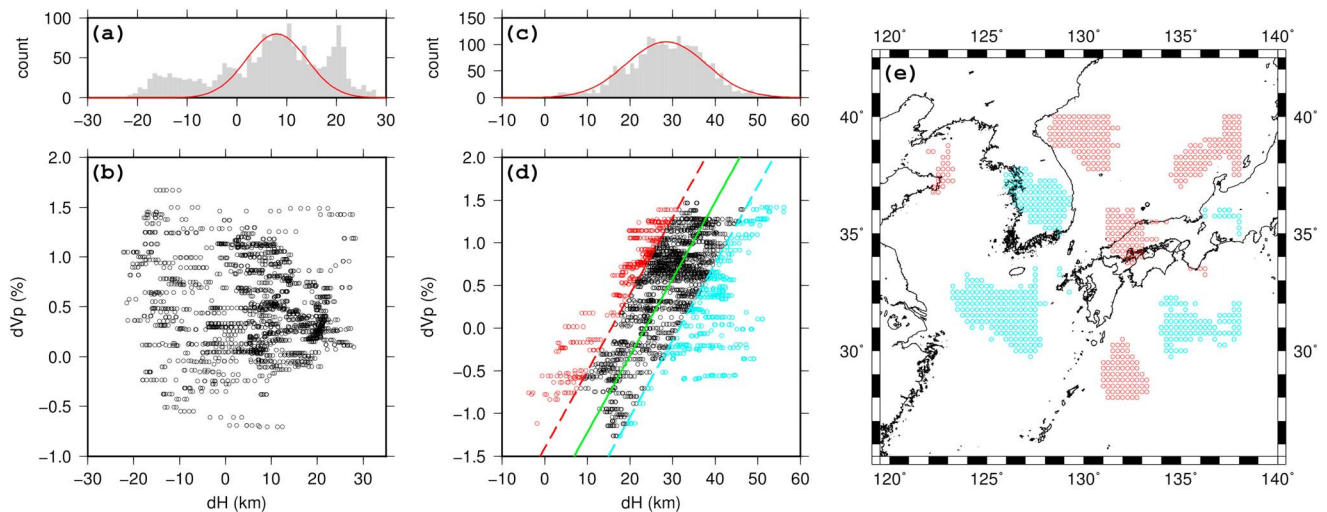
Figure 4. (a) Histogram of the dH (depth variation) of the 410 shown as gray bars with best fitting normal distribution in red line. (b) The distribution of the dV_P versus dH of the 410. (c and d) Same as Figures 4a and 4b, but for the 660. The green line represents the best fitting line with Clapeyron slope of −2.5 MPa/K, and the dashed lines represent the standard deviation (sigma) of the data distribution. Red and cyan circles indicate the scatters falling outside of the ± 1 sigma error bounds. (e) The geographic locations of the same scatters shown in Figure 4d. All data used in this figure are the same as ones in Figures 3d, 3e, 3g, and 3h.

important to understand the nature of the discontinuities, we set aside these observations for future study and instead focus on the topography of the 410 and the 660 in this study.

3. Results and Discussion

Figure 2 shows the CCP stacked receiver functions, along the profiles indicated in Figure 1. To emphasize the significant peaks, positive amplitudes of up to 2 sigma error bounds (negative side) from the mean are shaded in black. The mean and 2 sigma error bounds are derived from bootstrapping. To compare seismic velocity structure and receiver function results, we overlaid P wave velocity perturbations that were taken from the GAP-P2 model [*Obayashi et al.*, 2009], on a background image. Overall, positive peaks are clearly observed at depths corresponding to the 410 and the 660. In the profiles BB' and CC' (Figure 2), the 410 is elevated where it is penetrated by the cold Pacific slab, whereas the 660 is depressed where the slab reaches a depth of 660 km. However, the topographic maps of the 410 and the 660 (Figures 3a–3c) show features that are more complex in terms of depth variations of the upper mantle discontinuities. The mean depths of the 410 and the 660 are 415 and 677.4 km with standard deviations of 10.3 and 9 km, respectively. Far from the subducting slab, where the velocity perturbation is not strong, the depths of the discontinuities approach global average values. Therefore, we assume that the normal depths of the discontinuities in the study area are the same as global average depths. It is widely accepted that the velocity perturbations in the tomography model represent temperature changes. Therefore, it is interesting to compare depth changes and velocity changes (Figure 3). For a more quantitative comparison, the distribution of the velocity anomaly (dV_P) versus the depth change (dH) for the 410 (Figure 4b) and the 660 (Figure 4d) is investigated. For the 410, it is apparent that the correlation is very poor (Figure 4b), which indicates that depth changes are not controlled primarily by temperature changes. Conversely, the theoretical linear relationship derived from the Clapeyron slope of −2.5 MPa/K explains the main trend of the distribution for the 660 reasonably well, other than for some significant scatters (Figure 4d). Significant scatters clustered in specific regions (Figure 4e), and depth changes within those regions, might require alternative explanations besides temperature changes.

The IASP91 [*Kennett and Engdahl*, 1991], i.e., the 1-D reference Earth model, is widely known as a good reference model for imaging the upper mantle velocity structure. Furthermore, it has frequently been used to map amplitudes of phases to their corresponding conversion points—by using theoretically calculated arrival times —for the purpose of CCP stacking of receiver functions [e.g., *Cao and Levander*, 2010; *Tian et al.*, 2011; *Tauzin et al.*, 2013; *Li et al.*, 2013b]. However, a major drawback of this model is that it cannot account for the lateral heterogeneities of the Earth. Therefore, a 3-D model of the upper mantle velocity structure was also constructed, by combining the CRUST2.0 [*Bassin et al.*, 2000] and the GAP-P2 [*Obayashi et al.*, 2009] models.
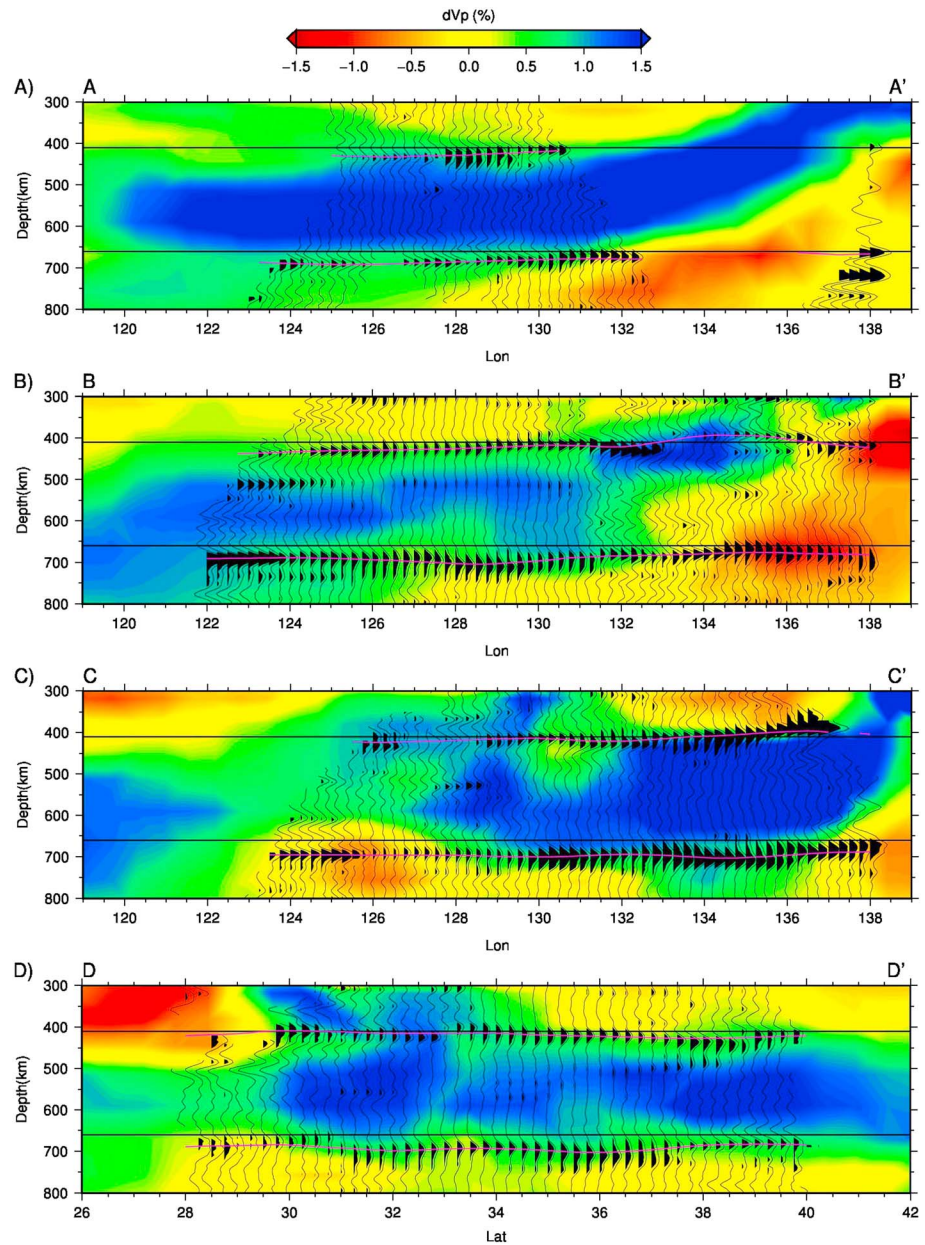
Figure 5. CCP stacked receiver function sections based on the 3-D velocity model constructed from CRUST2.0 and GAP-P2 for profile lines AA'–DD'. The positive amplitudes of up to 2 sigma error bounds from the mean are shaded in black. The mean and 2 sigma error bounds are derived from bootstrapping. The background color spectrum from blue to red represents fast to slow P wave velocity structure anomalies, respectively, from the GAP-P2 model [*Obayashi et al.*, 2009].

By comparing results produced by the IASP91 1-D model (Figures 2 and 3a–3c) with those produced by the 3-D model (Figures 5 and 3g–3i), the effects of heterogeneities of the Earth can be taken into account. Figure 5 shows the CCP stacked receiver functions obtained with the 3-D velocity model along profile lines AA'–DD' (Figure 1). Again, the observed depth changes of the 410 and the 660 are likely to have been the result of the low temperature of the cold Pacific Plate (Figure 2). The 410 and the 660 are estimated to be deeper when the 3-D velocity model is used. Differences in depths based on the 1-D and 3-D models become apparent in the western part of the study area. In theory, discontinuity depths—i.e., depths of P-to-S conversion points—become greater as V_P becomes higher, or as the V_P/V_S ratio becomes lower in the reference model. Compared with the IASP91 model, higher P wave velocities (V_P) above the 410 km depth of the GAP-P2 model can result in greater depths of both the 410 and the 660. In this study, the V_P/V_S ratio is held
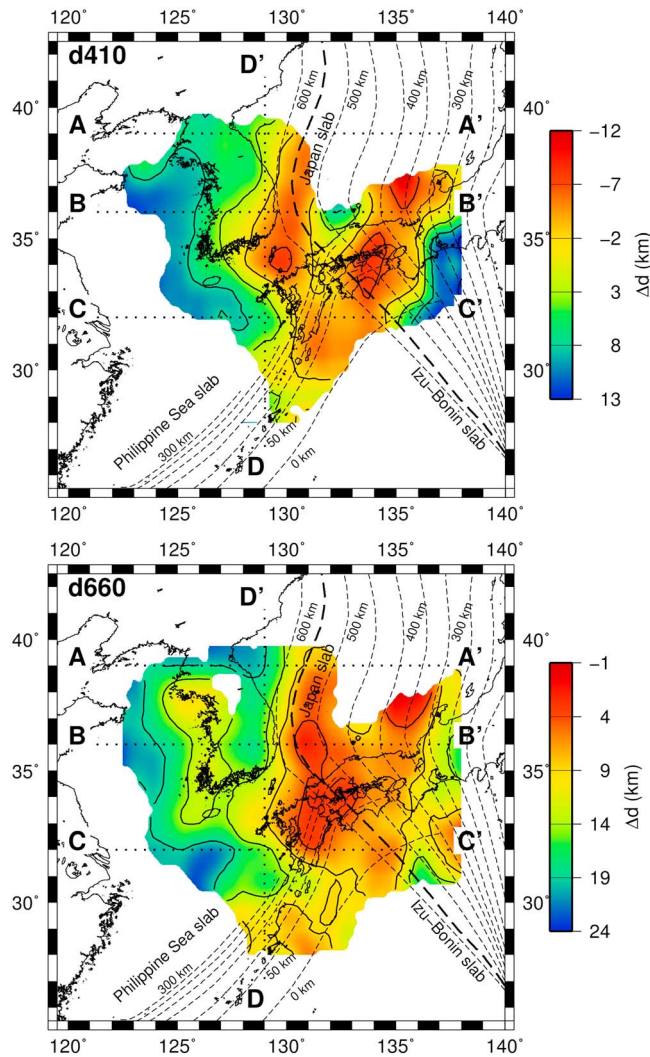
Figure 6. Differences between the topographic results obtained with the 1-D and 3-D models for (top) the 410 and (bottom) the 660.

fixed (at a value of 1.8) to facilitate construction of a 3-D velocity model. At this point it must be emphasized that recently, a higher water content was reported in the MTZ of the northwestern Pacific subduction zone [*Li et al.*, 2013a]. In the case of higher water content, a V_P/V_S ratio higher than 1.8 would be expected. Therefore, the depression of the 660 may be overestimated in this study. Figures 3g–3i show the topography of the 410 and the 660 based on the 3-D velocity model, similar to Figures 3a–3c.

Comparing Figures 3g–3i with Figures 3a–3c, the absolute depths of discontinuities are different. The difference between the topographic results obtained with the 1-D and 3-D models is shown in Figure 6. The difference maps for the 410 and the 660 show consistent patterns. This indicates that the velocity structure above the 410 is more important for the 3-D correction in this region. Although the difference between 1-D and 3-D corrections is not negligible, observed features in both topographic maps are generally consistent regardless of the reference model. Hence, it is unlikely that the observed lateral depth variation of the upper mantle discontinuities has been caused by the velocity model used for migration of receiver functions.

Three major anomalous features are identified from the topography of the 410 in the study area. First, an elevation of the 410 is observed where the cold subducting slab penetrates and passes through it, commonly associated with the positive Clapeyron slope of the olivine-to-wadsleyite transition. Many researchers have reported that the 410 beneath Japan is elevated by the effect of the cold Pacific slab [e.g., *Tono et al.*, 2005]. This elevation of the 410 has also been reported by receiver function studies [*Niu et al.*, 2005; *Tonegawa et al.*, 2005]. However, *Li et al.* [2000] did not detect the elevation of the 410, although they used a methodology identical to our own. According to *Li et al.* [2000], this could be explained by the issue of steep depth change, which could not be resolved in this narrow region of the elevated 410, due to low resolution resulting from the larger size of the stacking bin used in their study. Our results show features that are more detailed. If we look into the pattern of the elevated 410 shown in Figure 3a, the width of the elevated 410 becomes minimal—i.e., narrowest—around a latitude of 35°N, where tearing of the subducting slab has been reported by *Obayashi et al.* [2009]. This could indicate that our study has detected the gap of the torn subducting slab, where the 410 might not be elevated. However, this feature is not clear in the topographic map produced with the 3-D velocity model, due to the limited resolution of the receiver functions, and the spatial moving average used in this study. Therefore, we cannot rule out the possibility of an artifact. To ensure detection of the gap of the torn slab, a more detailed investigation is required. While the subducting Pacific Plate penetrates the 410 and descends into the MTZ, the Philippine Sea slab—subducting at the Ryukyu Trench—was also found to either reach or penetrate the 410 by *Abdelwahed and Zhao* [2007].

From the background tomography images along the profiles CC' and DD' (Figures 2c and 2d), high-velocity anomalies presumably caused by the Philippine Sea slab are observed above the 410. However, corresponding depth changes of the 410 were not observed in this study. This could imply that the Philippine Sea slab does not extend down as far as the 410, i.e., no temperature anomaly exists. However, it could also imply that the Philippine Sea slab does reach the 410, but that it is too thin and not cold enough for any changes in depth of the 410 to be observable, because of its young age.

The second anomalous feature is the significantly depressed 410 around (37°N, 138°E). This depression of the 410 is observed in both topographic maps, obtained from the 1-D velocity reference model and the 3-D velocity model. A low-velocity anomaly has been reported to exist atop this region of depression by many other tomographic studies [Bijwaard et al., 1998; Fukao et al., 2001; Zhao, 2004; Obayashi et al., 2006]. Zhao [2004] performed high-resolution travel time tomography, using both local and teleseismic events recorded by dense seismic networks on the Japanese Islands, to investigate the details of the low-velocity anomaly beneath the subducting Pacific slab. Based on the resultant high-resolution tomographic images, two possible explanations have been proposed for the anomaly. One explanation involves a local mantle convection pattern —a hot upwelling—induced by the subducting Pacific slab. The other explanation is that the anomaly might be a trace of a small mantle plume, rising upward from the lower mantle. Unfortunately, it is unclear which of these two explanations for the anomaly is more likely to be true. Two studies that used triplicated P waveforms [Obayashi et al., 2006] and multiple ScS reverberations [Bagley et al., 2009], respectively, have also been performed (in the region including the anomalous area). In both studies, a low-velocity layer was observed above the 410. However, the study that used triplicated P waveforms reported the observation of a depressed 410, while results of the multiple ScS reverberation study suggested an elevated 410. Although further investigations are required to reconcile these seemingly contradicting results, the depressed 410 observed in this study seems to be consistent with that observed in the triplicated P waveform study.

The last anomalous feature of the 410 in the study area is the broad depression stretching from the Korean Peninsula to Kyushu Island. The histogram for the depth of the 410 shows an interesting feature (Figure 4a). The overall histogram seems to follow the normal distribution, but there is a significant peak around the depth of 430 km. The geographic points corresponding to this depth are well correlated with the broadly depressed region. The most common explanation for this broad depression is that the temperature of this region is higher than that of surrounding regions. However, any evidence of low-velocity anomalies indicating high temperatures is not reported by tomography results [Obayashi et al., 2009]. The depression of the 410 might be an artifact that originated from low-velocity anomalies at the upper mantle—i.e., shallower than 300 km—in the study area [e.g., Fukao et al., 1992, 2009; Obayashi et al., 2006; Zhao et al., 2013], except where the subducting slab exists. These low-velocity anomalies at the upper mantle result in artificial depressions when the IASP91 1-D global average model is used, which is faster than the real earth. However, the coherency of the lateral velocity structure and 410 depression patterns has been found to be poor. Therefore, it is not likely that the depression of the 410 resulted from variations in temperature alone or that it is merely an artifact due to shallower low-velocity anomalies. In addition to variations in temperature, variations in chemical composition could also result in depth variations of the 410. For example, Schmerr and Garnero [2007] observed a seismic discontinuity at a depth that was somewhat deeper than the global average of the 410, extending several thousands of kilometers to the east of the Nazca slab subducting underneath the South American continent. They suggested the observed discontinuity to be the lower boundary of a hydrated lens of wadsleyite, rather than an olivine-to-wadsleyite transition boundary. Furthermore, they suggested that if it were an olivine-to-wadsleyite transition boundary, then Mg enrichment in the mantle wedge resulted in the observed depression of the 410. They also suggested that the large lateral extent—from east to west—of the depression might be related to trench rollback history.

East of the study area (Figure 1a), the Pacific Plate subducts westward. The subduction angle is gentle at the Japan Trench, becoming steeper toward the Izu-Bonin Trench. This spatial variation in the subduction angle originates from complex trench rollback history, including the opening of the East Sea [Miller and Kennett, 2006]. In Figure 3a, the width of the depressed 410 varies with latitude in a way similar to the angles of subduction. This indicates that discontinuity formation at depths below 410 km—beyond the subducting slab—by trench rollback migration might be possible, in a way similar to that suggested by Schmerr and Garnero [2007]. The variation of width of the 410 with latitude is not prominently visible in the map constructed using the 3-D velocity model. However, the depression of the 410 beneath the Korean Peninsula and Kyushu Island is clearly visible (Figure 3g).

That the Pacific slab has become stagnant after reaching the 660 has been imaged by many tomographic models [*Fukao et al.*, 2001; *Huang and Zhao*, 2006; *Obayashi et al.*, 2009]. For most regions in the study area, the cold slab could be expected to be atop the 660, except for those regions where the slab might have locally descended into the lower mantle. If we assume that the petrological and chemical compositions of the slab are uniform over the study area, temperature variations at the 660 should be the dominant cause for variations of its depth. If we only consider the effect of temperature, we might expect maximized depression where it is encountered by the slab. Furthermore, we might expect a gentle westward decrease of the level of depression, as the temperature difference between the slab and the surrounding mantle decreases [*Li et al.*, 2013a]. However, at points where the slab penetrates the 660 and descends into the lower mantle, local depressions can occur because the temperature at the center of the slab is lower than at its outer parts [*Li and Yuan*, 2003].

It is clear from Figure 2 that the 660 is considerably depressed at longitudes 130°E and 135°E in profile lines BB' and CC', respectively, and that these regions roughly correspond to those regions where the slab encounters it. Furthermore, the level of depression slowly decreases westward, and Figure 5 shows similar features. Although these observations are more or less consistent with expectations, the topographic maps of the 660 show complex features (Figures 3b and 3h). Based on the assumption that the thickness of the subducting slab is about 100 km, the 550-km contour line of the slab surface roughly indicates where the slab encounters the 660 and starts to affect the depth of the 660. Since the temperature of the slab is more or less uniform along the 550-km contour line, it is interesting to investigate depth variations of the 660 along the 550-km contour line, because along such lines, other depth-affecting factors might be most easily revealed. Interestingly, the depth of the 660 shows significant variation with latitude along the 550-km contour line. The most remarkable observation is that the depressed region of the 660 extends in the NW–SE direction along the 550-km contour line on the southeastern part of the study area. However, depression of the 660 does not appear at latitudes above 38°N. This pattern is consistent for both maps obtained using different reference models (Figures 3b and 3h).

Southeast of the study area, depressed regions of the 660 might be expected along the 550-km contour line because of the subducting cold Pacific slab associated with the Izu-Bonin Trench. Local maxima of depression have been observed underneath Kyushu Island and the northern Philippine Sea. Among these maxima, the significant depression underneath the northern Philippine Sea at 31°N, 135°E coincides with a high-velocity anomaly at a depth of ~660 km, reported by tomographic studies [*van der Hilst et al.*, 1991; *Fukao et al.*, 1992; *Obayashi et al.*, 2006]. Using the receiver functions obtained from Ocean Bottom Seismograph stations deployed in this area, the average depth of the 660 under the stagnant slab is reported to be 691 km [*Suetsugu et al.*, 2010]. Furthermore, the preferred 1-D velocity model for determining upper mantle structure—identified by using P wave triplications observed slightly south of the high-velocity anomaly—shows a depression of approximately 30 km [*Shito and Shibutani*, 2001]. However, another such 1-D velocity model constructed using P wave triplications for a region west of the high-velocity anomaly observed in this study [*Brudzinski et al.*, 1997; *Tseng and Chen*, 2004] indicates a high-velocity layer above the 660, while there are no depth changes of the 660. Results obtained using P wave triplications provide local characteristics of the seismic velocity structure, where seismic phases are either refracted or reflected at discontinuities. Therefore, the different results obtained for adjacent regions indicate that the depth of the 660 fluctuates significantly beneath the stagnant slab. P wave triplication studies have also produced various results about the 660 beneath Kyushu where the locally depressed 660 is observed in this study [*Shito and Shibutani*, 2001; *Tajima et al.*, 2009]. The variety of results from P wave triplication studies also indicates that the depth of the 660 changes rapidly beneath Kyushu Island, which supports the possibility of a large local depression. In our study, the depth of the 660 was observed to increase by more than 40 km at the local maximum. Under the assumption of a Clapeyron slope of −2.5 MPa/K [*Fukao et al.*, 2009], this implies that the temperature is ~650° lower at this maximum, compared with the surrounding mantle. If we account for the water content as well as the Clapeyron slope, the depth change of the 660 and the seismic velocity change are converted to the thermal change and the water content change [*Suetsugu et al.*, 2006]. The maximum depression of the 660 is 44 km, and the velocity perturbation at the same location is 1.4%. Thus, the thermal change of −690 K and water content change of 1.1 wt % are derived. This difference in temperature indicates the possibility of the slab penetrating the 660 and descending into the lower mantle. This is further supported by the high-velocity anomaly observed at a depth of 756 km, through the tomographic model of *Obayashi et al.* [2009].

As was mentioned earlier, the depth of the 660 along the 550-km contour line has local maxima to the south of the study area, elevating with increasing latitude. Furthermore, the depression of the 660 becomes less than 20 km—eventually—at latitudes above 38°N, which is consistent with previous studies that also report weak depression beneath the east coast of the central Korean Peninsula. This region of undepressed 660 is well correlated with one of the locations where dH is not correlated with dV_P (Figure 4). *Li et al.* [2000] reported a depression of the 660 in the latitude range of 30°N–45°N. Meanwhile, they observed that the 660 was not depressed beneath the central part of the Korean Peninsula (refer to Figures 8c and 8d in *Li et al.* [2000]). However, they have not explained why the 660 is not depressed at these latitudes. When compared in detail, our results show different features than those of *Li et al.* [2000], due to differences in resolution. However, the undepressed 660 beneath the east coast of the Korean Peninsula was consistently revealed by both this study and *Li et al.* [2000]. Other evidence that the 660 is not depressed is presented by *Tajima et al.* [2009], who identified the preferred seismic 1-D velocity models for determining upper mantle structure beneath northeast Asia, by performing *P* wave triplication studies. Their models consistently showed a high-velocity layer above the 660, indicating the stagnant slab from latitudes 30°N–45°N, along the 550-km contour line. Furthermore, they found the 660 to be depressed at latitude 37°N, but not between latitudes 39°N and 40°N. According to these diverse studies, it is likely that the 660 is not depressed in the latter region. There are several possible explanations for this phenomenon, despite the presence of the cold stagnant slab.

One possible explanation is the absence of the stagnant slab in this particular area. However, this is very unlikely because of the occurrence of earthquakes at depths below 600 km and because of the high-velocity anomalies that have been reportedly observed above the 660 by many independent tomographic studies.

Another explanation is given by the possibility of a different petrological or geochemical composition of the slab in this particular area [*Tajima et al.*, 2009]. *Tajima et al.* [2009] suggested a hypothetical model of a hydrous garnet-rich layer, i.e., a layer of subducted crust at the uppermost part of the slab, flowing down to the 660 at the tip and the gap of the stagnant slab. This led them to interpret the undepressed 660 to be adjacent to the depressed 660. This model also explains the discrepancy between the depressed and undepressed 660, having in common a high-velocity layer above the 660. If this model were true, the topography should have features that show regions of the depressed 660 bounded by regions of the undepressed 660. However, no such features could be identified from our topographic maps.

A third possible explanation is offered by the possibility of changing water content in the slab. Recently, it has been reported that the depth of the postspinel transformation depends on water content [*Higo et al.*, 2001; *Yamada et al.*, 2009]. According to these studies, 2.0 wt % of water can cause the 660 to depress by about 15 km without temporal change [*Cao and Levander*, 2010]. Moreover, *Litasov et al.* [2005] revealed that the Clapeyron slope of the postspinel transformation varies significantly with water content. They determined the Clapeyron slope to be −0.5 MPa/K for an anhydrous mantle and −2.0 MPa/K for a hydrous mantle with 2.0 wt % of water. Furthermore, they found that the depth of the postspinel transformation could increase by as much as 30 km in the hydrous mantle, as opposed to only 7.5 km in the anhydrous mantle (under identical temperature conditions). According to these results, even under the condition of homogenous temperature, the 660 depth might vary with water content. Therefore, the depth variations of the 660 that occur under the conditions of homogenous temperature along the 550-km contour line might indicate water content heterogeneity—in the slab or MTZ—beneath the study area. However, the origins of the differences in water content remain unclear, and studies that are more comprehensive are required to investigate this.

Last, the depth change of the 660 could be a consequence of differences in complex geodynamical properties, such as subduction angles, or undulation of slabs. The location where the depth of the 660 changes rapidly along the 550-km contour line is close to the boundary between the two subducting slabs associated with the Japan Trench and the Izu-Bonin Trench (if we project the boundary at the junction of the trenches at the ocean floor to a depth of 660 km, based on the assumption that the directions of subduction are uniform). This indicates that differences in depth of the 660 might be related to the characteristics of the slabs subducting at the Japan Trench and the Izu-Bonin Trench. The Japan slab subducts with an inclination of 30° [*Miller and Kennett*, 2006] and a convergence rate of 9.2 cm/yr [*DeMets et al.*, 1994], and the Izu-Bonin slab subducts with an inclination of 45° [*Miller and Kennett*, 2006] and a convergence rate of about 6 cm/yr [*Seno et al.*, 1993]. This difference in the angle of subduction of these two slabs in the northwestern Pacific, which has been attributed to the complex trench rollback history [*Miller and Kennett*, 2006], has also been identified by the tomographic models (Figure 2). The geometrical properties of subducting slabs descending into the MTZ are determined by

their angles of subduction and their convergence rates. In general, when the subduction angle is high, slabs penetrate the 660 and descend into the lower mantle. When the subduction angle is low, slabs do not penetrate the 660 but deform and bend, prior to becoming stagnant. The Japan slab and Izu-Bonin slab are generally considered stagnant above the 660. However, their different geometrical properties could result in—locally—distinct geometries of these stagnant slabs. In turn, this could lead to depth variations of the 660 along the 550-km contour line.

4. Conclusions

To understand the interactions between the subducting Pacific slab and the upper mantle discontinuities, we investigated the topography of the 410 and the 660 using teleseismic receiver functions recorded by seismic stations in the Korean Peninsula and southwestern Japan. We used 1-D and 3-D velocity models to migrate receiver functions to piercing (conversion) points of *P*-to-*S* converted phases, and CCP stacking techniques were applied to construct images of the upper mantle discontinuities. Peaks corresponding to the 410 and the 660 were observed consistently between the 1-D and 3-D velocity models used for migration of receiver functions and clearly imaged for the entire area of study, while for some regions multiple peaks were observed. The images confirm that the regional topography of the 410 and the 660 are affected by the subducting slab. Moreover, the lateral variations of the depths of both discontinuities are highly complex and cannot be explained by variations in temperature alone. In general, the 410 and the 660 are elevated and depressed, respectively, where there are subducting cold slabs. The region of the depressed 410 observed beneath the Korean Peninsula and southwestern Japan might indicate a type of relict structure related to the complex trench rollback history of the region. For the 660, it is well known that the slab becomes stagnant in this region. However, a considerable depression of the 660 is locally observed in the northern Philippine Sea, which might indicate that the subducting slab could penetrate the 660 and descend toward the lower mantle at certain locations. The most important finding of this study is that the depth of the 660 varies systematically along the trench axis. Possibly, this is simply because the angle of subduction varies with latitude, although the spatial heterogeneity of water content of the slabs might also contribute to this effect. It is an interesting hypothesis, but we still need to explain how water content could be heterogeneous at this depth.

References

Abdelwahed, M. F., and D. Zhao (2007), Deep structure of the Japan subduction zone, *Phys. Earth Planet. Inter.*, *162*(1–2), 32–52, doi:10.1016/j.pepi.2007.03.001.

Ai, Y., and T. Zheng (2003), The upper mantle discontinuity structure beneath eastern China, *Geophys. Res. Lett.*, *30*(21), 2089, doi:10.1029/2003GL017678.

Ai, Y., T. Zheng, W. Xu, Y. He, and D. Dong (2003), A complex 660 km discontinuity beneath northeast China, *Earth Planet. Sci. Lett.*, *212*(1–2), 63–71, doi:10.1016/S0012-821X(03)00266-8.

Bagley, B., A. M. Courtier, and J. Revenaugh (2009), Melting in the deep upper mantle oceanward of the Honshu slab, *Phys. Earth Planet. Inter.*, *175*(3–4), 137–144, doi:10.1016/j.pepi.2009.03.007.

Bassin, C., G. Laske, and G. Masters (2000), The current limits of resolution for surface wave tomography in North America, *Eos Trans. AGU*, *81*, F897.

Bijwaard, H., W. Spakman, and E. R. Engdahl (1998), Closing the gap between regional and global travel time tomography, *J. Geophys. Res.*, *103*, 30,055–30,078, doi:10.1029/98JB02467.

Brudzinski, M., W. Chen, R. Nowack, and B. Huang (1997), Variations of *P* wave speeds in the mantle transition zone beneath the northern Philippine Sea, *J. Geophys. Res.*, *102*, 11,815–11,827, doi:10.1029/97JB00212.

Cao, A., and A. Levander (2010), High-resolution transition zone structures of the Gorda Slab beneath the western United States: Implication for deep water subduction, *J. Geophys. Res.*, *115*, B07301, doi:10.1029/2009JB006876.

DeMets, C., R. G. Gordon, D. F. Argus, and S. Stein (1994), Effect of recent revisions to the geomagnetic reversal time scale on estimates of current plate motions, *Geophys. Res. Lett.*, *21*, 2191–2194, doi:10.1029/94GL02118.

Fukao, Y., M. Obayashi, H. Inoue, and M. Nenbai (1992), Subducting slabs stagnant in the mantle transition zone, *J. Geophys. Res.*, *97*, 4809–4822, doi:10.1029/91JB02749.

Fukao, Y., S. Widiyantoro, and M. Obayashi (2001), Stagnant slabs in the upper and lower mantle transition region, *Rev. Geophys.*, *39*, 291–323, doi:10.1029/1999RG000068.

Fukao, Y., M. Obayashi, and T. Nakakuki (2009), Stagnant slab: A review, *Annu. Rev. Earth Planet. Sci.*, *37*(1), 19–46, doi:10.1146/annurev.earth.36.031207.124224.

Gudmundsson, O., and M. Sambridge (1998), A regionalized upper mantle (RUM) seismic model, *J. Geophys. Res.*, *103*, 7121–7136, doi:10.1029/97JB02488.

Higo, Y., T. Inoue, T. Irifune, and H. Yurimoto (2001), Effect of water on the spinel-postspinel transformation in Mg2SiO4, *Geophys. Res. Lett.*, *28*, 3505–3508, doi:10.1029/2001GL013194.

Huang, J., and D. Zhao (2006), High-resolution mantle tomography of China and surrounding regions, *J. Geophys. Res.*, *111*, B09305, doi:10.1029/2005JB004066.

Ita, J., and L. Stixrude (1992), Petrology, elasticity, and composition of the mantle transition zone, *J. Geophys. Res.*, *97*, 6849–6866, doi:10.1029/92JB00068.

Ito, E., and E. Takahashi (1989), Postspinel transformations in the system Mg2SiO4-Fe2SiO4 and some geophysical implications, *J. Geophys. Res.*, *94*, 10,637–10,646, doi:10.1029/JB094iB08p10637.

Kennett, B. L. N., and E. R. Engdahl (1991), Traveltimes for global earthquake location and phase identification, *Geophys. J. Int.*, *105*(2), 429–465, doi:10.1111/j.1365-246X.1991.tb06724.x.

Li, J., X. Wang, X. Wang, and D. A. Yuen (2013a), *P* and *SH* velocity structure in the upper mantle beneath Northeast China: Evidence for a stagnant slab in hydrous mantle transition zone, *Earth Planet. Sci. Lett.*, *367*, 71–81, doi:10.1016/j.epsl.2013.02.026.

Li, Q., R. Gao, F. T. Wu, Y. Guan, Z. Ye, Q. Liu, H. Kuo-Chen, R. He, W. Li, and X. Shen (2013b), Seismic structure in the southeastern China using teleseismic receiver functions, *Tectonophysics*, *606*, 24–35, doi:10.1016/j.tecto.2013.06.033.

Li, X., and X. Yuan (2003), Receiver functions in northeast China—Implications for slab penetration into the lower mantle in northwest Pacific subduction zone, *Earth Planet. Sci. Lett.*, *216*(4), 679–691, doi:10.1016/S0012-821X(03)00555-7.

Li, X., S. V. Sobolev, R. Kind, X. Yuan, and C. Estabrook (2000), A detailed receiver function image of the upper mantle discontinuities in the Japan subduction zone, *Earth Planet. Sci. Lett.*, *183*(3–4), 527–541, doi:10.1016/S0012-821X(00)00294-6.

Ligorria, J. P., and C. J. Ammon (1999), Iterative deconvolution and receiver-function estimation, *Bull. Seismol. Soc. Am.*, *89*, 1395–1400.

Litasov, K. D., E. Ohtani, A. Sano, A. Suzuki, and K. Funakoshi (2005), Wet subduction versus cold subduction, *Geophys. Res. Lett.*, *32*, L13312, doi:10.1029/2005GL022921.

Matsumoto, T., Y. Ito, H. Matsubayashi, and S. Sekiguchi (2006), Spatial distribution of F-net moment tensors for the 2005 West Off Fukuoka Prefecture Earthquake determined by the extended method of the NIED F-net routine, *Earth Planets Space*, *58*, 63–67.

Mégnin, C., and B. Romanowicz (2000), The three-dimensional shear velocity structure of the mantle from the inversion of body, surface and higher-mode waveforms, *Geophys. J. Int.*, *143*, 709–728, doi:10.1046/j.1365-246X.2000.00298.x.

Miller, M. S., and B. L. N. Kennett (2006), Evolution of mantle structure beneath the northwest Pacific: Evidence from seismic tomography and paleogeographic reconstructions, *Tectonics*, *25*, TC4002, doi:10.1029/2005TC001909.

Morishima, H., T. Kato, M. Suto, E. Ohtani, S. Urakawa, W. Utsumi, O. Shimomura, and T. Kikegawa (1994), The phase boundary between α- and β-Mg2SiO4 determined by in situ X-ray observation, *Science*, *265*(5176), 1202–1203, doi:10.1126/science.265.5176.1202.

Niu, F., A. Levander, S. Ham, and M. Obayashi (2005), Mapping the subducting Pacific slab beneath southwest Japan with Hi-net receiver functions, *Earth Planet. Sci. Lett.*, *239*(1–2), 9–17, doi:10.1016/j.epsl.2005.08.009.

Obayashi, M., H. Sugioka, J. Yoshimitsu, and Y. Fukao (2006), High temperature anomalies oceanward of subducting slabs at the 410-km discontinuity, *Earth Planet. Sci. Lett.*, *243*(1–2), 149–158, doi:10.1016/j.epsl.2005.12.032.

Obayashi, M., J. Yoshimitsu, and Y. Fukao (2009), Tearing of stagnant slab, *Science*, *324*(5931), 1173–1175, doi:10.1126/science.1172496.

Owens, T. J., A. A. Nyblade, H. Gurrola, and C. A. Langston (2000), Mantle transition zone structure beneath Tanzania, East Africa, *Geophys. Res. Lett.*, *27*, 827–830, doi:10.1029/1999GL005429.

Park, Y., S. C. Park, K. H. Kim, M. Park, and J. Lee (2010), Magnitude scaling relationships from the first 3 s of *P*-wave arrivals in South Korea, *J. Seismol.*, *14*, 761–768, doi:10.1007/s10950-010-9198-3.

Ringwood, A. E. (1975), *Composition and Petrology of the Earth's Mantle*, McGraw-Hill, New York.

Ringwood, A. E. (1994), Role of the transition zone and 660 km discontinuity in mantle dynamics, *Phys. Earth Planet. Inter.*, *86*(1–3), 5–24, doi:10.1016/0031-9201(94)05058-9.

Schmerr, N., and E. J. Garnero (2007), Upper mantle discontinuity topography from thermal and chemical heterogeneity, *Science*, *318*(5850), 623–626, doi:10.1126/science.1145962.

Seno, T., S. Stein, and A. E. Gripp (1993), A model for the motion of the Philippine Sea Plate consistent with NUVEL-1 and geological data, *J. Geophys. Res.*, *98*, 17,941–17,948, doi:10.1029/93JB00782.

Shearer, P. M. (1996), Transition zone velocity gradients and the 520-km discontinuity, *J. Geophys. Res.*, *101*, 3053–3066, doi:10.1029/95JB02812.

Shearer, P. M., and T. G. Masters (1992), Global mapping of topography on the 660-km discontinuity, *Nature*, *355*(6363), 791–796, doi:10.1038/355791a0.

Shito, A., and T. Shibutani (2001), Upper mantle transition zone structure beneath the Philippine Sea region, *Geophys. Res. Lett.*, *28*, 871–874, doi:10.1029/2000GL012235.

Simmons, N. A., and H. Gurrola (2000), Multiple seismic discontinuities near the base of the transition zone in the Earth's mantle, *Nature*, *405*, 559–562.

Song, T.-R. A., D. V. Helmberger, and S. P. Grand (2004), Low-velocity zone atop the 410-km seismic discontinuity in the northwestern United States, *Nature*, *427*(6974), 530–533, doi:10.1038/nature02231.

Suetsugu, D., T. Inoue, A. Yamada, D. Zhao, and M. Obayashi (2006), Towards mapping the three-dimensional distribution of water in the transition zone from *P*-velocity tomography and 660-km discontinuity depths, *Geophys. Monogr. Ser.*, vol. 168, edited by S. D. Jacobsen and S. van der Lee, pp. 237–249, AGU, Washington, D. C.

Suetsugu, D., et al. (2010), Depths of the 410-km and 660-km discontinuities in and around the stagnant slab beneath the Philippine Sea: Is water stored in the stagnant slab?, *Phys. Earth Planet. Inter.*, *183*(1–2), 270–279, doi:10.1016/j.pepi.2010.09.004.

Tajima, F., I. Katayama, and T. Nakagawa (2009), Variable seismic structure near the 660 km discontinuity associated with stagnant slabs and geochemical implications, *Phys. Earth Planet. Inter.*, *172*(3–4), 183–198, doi:10.1016/j.pepi.2008.09.013.

Tauzin, B., R. D. van der Hilst, G. Wittlinger, and Y. Ricard (2013), Multiple transition zone seismic discontinuities and low velocity layers below western United States, *J. Geophys. Res. Solid Earth*, *118*, 2307–2322, doi:10.1002/jgrb.50182.

Tian, X., J. Teng, H. Zhang, Z. Zhang, Y. Zhang, H. Yang, and K. Zhang (2011), Structure of crust and upper mantle beneath the Ordos Block and the Yinshan Mountains revealed by receiver function analysis, *Phys. Earth Planet. Inter.*, *184*(3–4), 186–193, doi:10.1016/j.pepi.2010.11.007.

Tonegawa, T., K. Hirahara, and T. Shibutani (2005), Detailed structure of the upper mantle discontinuities around the Japan subduction zone imaged by receiver function analyses, *Earth Planets Space*, *57*, 5–14.

Tono, Y., T. Kunugi, Y. Fukao, S. Tsuboi, K. Kanjo, and K. Kasahara (2005), Mapping of the 410- and 660-km discontinuities beneath the Japanese islands, *J. Geophys. Res.*, *110*, B03307, doi:10.1029/2004JB003266.

Tseng, T.-L., and W.-P. Chen (2004), Contrasts in seismic wave speeds and density across the 660-km discontinuity beneath the Philippine and the Japan Seas, *J. Geophys. Res.*, *109*, B04302, doi:10.1029/2003JB002613.

Van der Hilst, R., R. Engdahl, W. Spakman, and G. Nolet (1991), Tomographic imaging of subducted lithosphere below northwest Pacific island arcs, *Nature*, *353*(6339), 37–43, doi:10.1038/353037a0.

Yamada, A., D. Zhao, T. Inoue, D. Suetsugu, and M. Obayashi (2009), Seismological evidence for compositional variations at the base of the mantle transition zone under Japan Islands, *Gondwana Res.*, *16*(3–4), 482–490, doi:10.1016/j.gr.2009.04.009.

Zhao, D. (2004), Global tomographic images of mantle plumes and subducting slabs: Insight into deep Earth dynamics, *Phys. Earth Planet. Inter.*, *146*(1–2), 3–34, doi:10.1016/j.pepi.2003.07.032.

Zhao, D., Y. Yamamoto, and T. Yanada (2013), Global mantle heterogeneity and its influence on teleseismic regional tomography, *Gondwana Res.*, *23*(2), 595–616, doi:10.1016/j.gr.2012.08.004.